presented at ASME Int. Gas Turbine and Aeroengine Cong., Orlando, June 1997 as paper 97-GT-243

FLOW IN A "COVER-PLATE" PRE-SWIRL ROTOR-STATOR SYSTEM

Hasan Karabay, Jian-Xin Chen, Robert Pilbrow
Michael Wilson and J Michael Owen

School of Mechanical Engineering
University of Bath
Bath BA2 7AY, UK

ABSTRACT

This paper describes a combined theoretical, computational and experimental study of the flow in an adiabatic pre-swirl rotor-stator system. Pre-swirl cooling air, supplied through nozzles in the stator, flows radially outward, in the rotating cavity between the rotating disc and a cover-plate attached to it, leaving the system through blade-cooling holes in the disc. An axisymmetric elliptic solver, incorporating the Launder-Sharma low-Reynolds-number k-ε turbulence model, is used to compute the flow. An LDA system is used to measure the tangential component of velocity, V_ϕ, in the rotating cavity of a purpose-built rotating-disc rig. For rotational Reynolds numbers up to 1.2×10^6 and pre-swirl ratios up to 2.5, agreement between the computed and measured values of V_ϕ is mainly very good, and the results confirm that free-vortex flow occurs throughout most of the rotating cavity. Computed values of the pre-swirl effectiveness (or the nondimensional temperature difference between the pre-swirl and blade-cooling air) agree closely with theoretical values obtained from a thermodynamic analysis of an adiabatic system.

NOMENCLATURE

b	outer radius of disc
c_p	specific heat at constant pressure
C_w	nondimensional flow rate ($m/\mu b$)
e_Θ	difference between computed and theoretical adiabatic effectiveness
k	turbulent kinetic energy
m	mass flow rate of cooling air
Ma	Mach number
r	radius
r_i, r_o	inner, outer radius of annular pre-swirl chamber
Re_ϕ	rotational Reynolds number ($\rho\Omega b^2/\mu$)
s	axial clearance between rotor and stator
T	static temperature
T_o	total temperature in stationary frame
T_t	total temperature in rotating frame
V_r , V_ϕ , V_z	radial, tangential and axial components of velocity in stationary frame
x	nondimensional radius (r/b)
z	axial distance from stator
β	swirl ratio ($V_\phi / \Omega r$)
γ	ratio of specific heats
ε	turbulent energy dissipation rate
Θ	adiabatic effectiveness (equation 7)
Θ'	ideal adiabatic effectiveness (equation 8)
λ_T	turbulent flow parameter ($C_w\, Re_\phi^{-0.8}$)
μ	dynamic viscosity
ρ	static density
ϕ	fraction of disc-cooling air that enters blade-cooling passages
Ω	angular speed of rotating disc

Subscripts

b	blade-cooling flow
d	disc-cooling flow
e	edge of source region
eff	effective value
0	value when $\beta_p = 0$
p,p′	pre-swirl flow, ideal pre-swirl flow
s	sealing flow or location of stagnation point
1	upstream of pre-swirl nozzles
1′	downstream of pre-swirl nozzles
2′	upstream of blade-cooling passages
2	inside blade-cooling passages

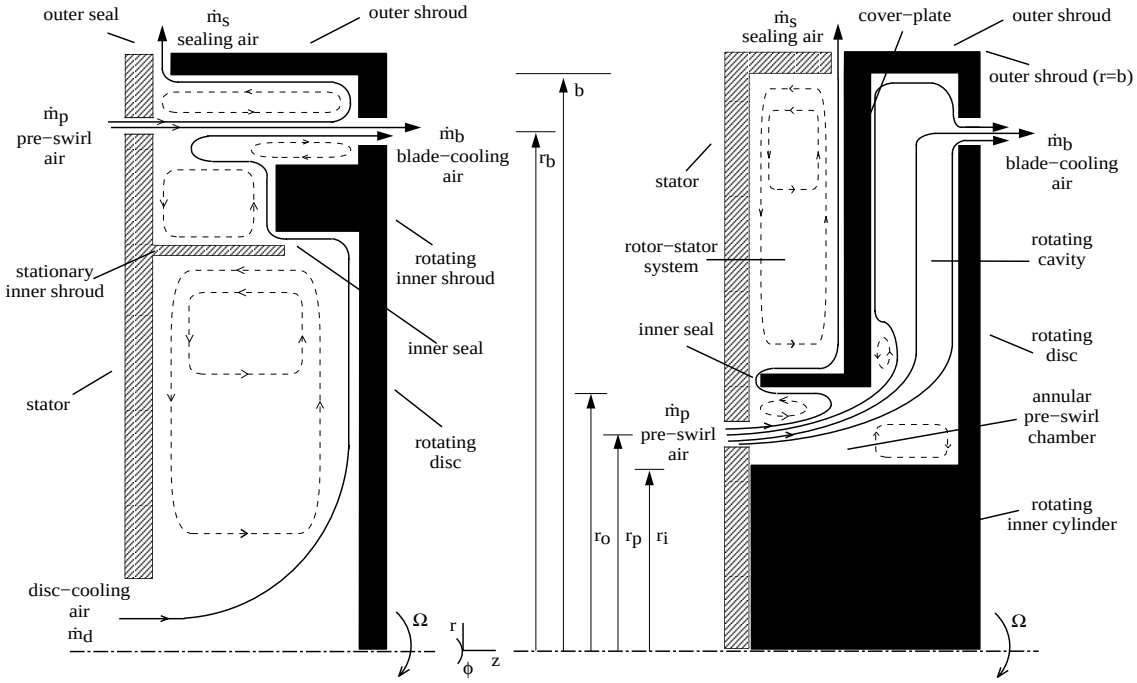

a) direct−transfer system b) cover−plate system

Fig. 1 Schematic diagram of pre−swirl systems

primary flow secondary flow rotating stationary

1 INTRODUCTION

Fig 1 shows a schematic diagram of two pre-swirl systems that are commonly used to supply cooling air to gas-turbine blades. In the so-called direct-transfer (or large-radius) system, the pre-swirl nozzles are located in a stationary casing, or stator, at a radial position, r_p, approximately equal to the inlet radius of the blade-cooling passages, r_b. In the cover-plate (or small-radius) system, the pre-swirl nozzles are located in the stator radially inward of the blade-cooling passages, and the air flows outward in the clearance between the turbine disc and a cover-plate attached to it.

By swirling the cooling air in the direction of rotation of the disc, the temperature of the air entering the blade-cooling passages is reduced. In both systems, air is used to remove the windage heating from the turbine disc and to provide a sealing flow to reduce the ingress of hot mainstream gas at the periphery of the system. For the direct-transfer system, most, or all, of the disc-cooling air and some of the ingested mainstream gas ends up in the blade-cooling passages. In the cover-plate system, an inner seal is used to prevent this undesirable contamination of blade-coolant with either disc-cooling air or ingested gas.

In the cover-plate system, a free vortex is created as the air flows radially outward in the rotating cavity between the disc and the cover-plate. For radial outflow in rotating cavities (see Owen and Rogers 1995), there is usually a source region near the inlet, where inviscid free-vortex flow occurs between two entraining boundary layers; radially outward of the source region, there is a core of inviscid rotating fluid (which is *not* a free vortex) between two nonentraining Ekman-type layers.

The radial extent of the source region depends principally on the pre-swirl ratio, β_p, of the incoming air and on the turbulent flow parameter, λ_T, where β_p and λ_T are defined in the Nomenclature. For sufficiently large values of λ_T, the source region fills the entire cavity; this is usually the case for the pre-swirl cooling systems considered here. Another feature of rotating cavities is that the flow in the boundary layers is radially outward when the inviscid core rotates slower than the discs, and it is radially inward when the core rotates faster. There is, therefore, a stagnation point in the boundary layer at the radial location where $V_\phi = \Omega r$ in the inviscid core.

Computational and experimental studies in pre-swirl systems, with and without heat transfer, have been conducted by a number of research workers, and the reader is referred to Meierhofer and Franklin (1981), El-Oun and Owen (1989), Chen, Owen and Wilson (1993a,b), Wilson, Pilbrow and Owen (1995) and Popp, Zimmermann and Kutz (1996). Details of the flow and heat transfer in rotor-stator systems in general, and the subject of ingress in particular, are given by Owen and Rogers (1989).

The work described here is concerned principally with an adiabatic pre-swirl cover-plate system. In Section 2, the performance of an adiabatic system is analysed, and expressions are derived for the pre-swirl effectiveness in both direct-transfer and cover-plate systems. The computational method and the experimental apparatus are described in sections 3 and 4, respectively, and the computational

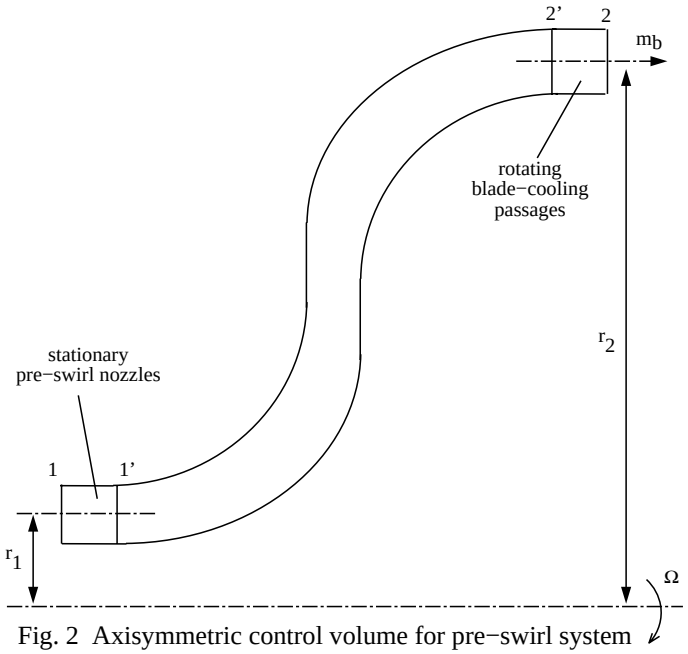

Fig. 2 Axisymmetric control volume for pre−swirl system

results and the experimental velocity measurements are discussed in Section 5. Conclusions are presented in Section 6.

2 ANALYSIS OF AN ADIABATIC PRE-SWIRL SYSTEM

2.1 Pre-swirl effectiveness

Fig 2 shows the control volume used in the analysis. Stations 1 and 1′ are respectively immediately upstream and downstream of the pre-swirl nozzles, and 2′ and 2 are respectively immediately upstream of and inside the blade-cooling passages; $r_{1'} = r_1$ and $r_{2'} = r_2$. From 1 to 2′ the flow is taken to be isentropic, and from 2′ to 2 work is done to adjust the tangential speed of the air, $V_{\phi 2'}$, to that of the disc, $V_{\phi 2}$.

From the first law of thermodynamics for an adiabatic open system, the rate of work done on the air is equal to the rate of increase of its total enthalpy. Also, as the air moves from stations 1′ to 2, the moment exerted by the rotating surfaces equals the rate of change of angular momentum of the air; the product of this moment and the angular speed of the disc is equal to the rate of work done on the air. Hence,

$$c_p (T_{02} - T_{01'}) = \Omega (r_2 V_{\phi 2} - r_{1'} V_{\phi 1'}) \quad (1)$$

or, as $T_{01'} = T_{01}$ and $V_{\phi 2} = \Omega r_2$,

$$c_p (T_{02} - T_{01}) = \Omega^2 r_2^2 \left[1 - \beta_{p'} \left(\frac{r_1}{r_2} \right)^2 \right] \quad (2)$$

where $\beta_{p'} = V_{\phi 1'} / \Omega r_1$ is the inlet pre-swirl ratio.

It should be noted that equation (2) is valid for viscid and inviscid flow providing all the blade-cooling air originates from the pre-swirl nozzles. This condition should always be true for the cover-plate system, but it will not be true for a direct-transfer system where the disc-cooling and blade-cooling flows mix, as shown in Fig 1. In fact, there is computational and experimental evidence (see El-Oun and Owen 1989 and et al 1993a, b) that, even when there are discrete blade-cooling holes rather than the annular slot considered here, most or all of the disc-cooling air ends up in the blade-cooling passages, and some of the pre-swirl air leaves the system through the peripheral seals.

It is convenient to define ϕ as the ratio of the disc-cooling air that enters the blade-cooling passages to the total flow that enters these passages. For the cover-plate system, $\phi = 0$; for the direct-transfer system it is assumed that $\phi = m_d/m_b$. If the disc-cooling air enters the system with zero swirl, equation (2) becomes

$$c_p (T_{02} - T_{01}) = \Omega^2 r_2^2 \left[1 - (1-\phi) \beta_{p'} \left(\frac{r_1}{r_2} \right)^2 \right] \quad (3)$$

(It should be noted that the effect of the disc-cooling air could be reduced if it were swirled at inlet to the system.)

Also,

$$c_p T_{02} = c_p T_2 \left(1 + \frac{\gamma - 1}{2} Ma_2^2\right) \quad (4)$$

$$= c_p T_2 + \tfrac{1}{2} (V_r^2 + V_\phi^2 + V_z^2)_2 \quad (5)$$

It is convenient to define T_{t2} as the total temperature in the rotating frame, which is the value that would be measured by a total-temperature probe inside a blade-cooling passage; it is this temperature that controls the heat transfer from the blade to the air. By definition

$$c_p T_{t2} = c_p T_2 + \tfrac{1}{2} V_{r2}^2 + \tfrac{1}{2} V_{z2}^2 \quad (6)$$

where, for normal blade-cooling passages, $V_{r2} = 0$.

It is also convenient to define the nondimensional pre-swirl effectiveness, Θ, as

$$\Theta = \frac{c_p (T_{01} - T_{t2})}{\frac{1}{2} \Omega^2 r_2^2} \quad (7)$$

which is the nondimensional difference in the total temperature between the stationary pre-swirl nozzles and the rotating blade-cooling passages. A positive value of Θ indicates that the pre-swirl system is effective in reducing the total temperature of the blade-cooling air.

Using equations (3), (5) and (6), it follows that the ideal effectiveness, Θ', is given by

$$\Theta' = 2(1-\phi) \beta_{p'} \left(\frac{r_1}{r_2} \right)^2 - 1 \quad (8)$$

For the direct-transfer system, where $\phi = m_d/m_b$ and $r_1 = r_2$,

$$\Theta' = 2\left(1 - \frac{m_d}{m_b}\right) \beta_{p'} - 1 \quad (9)$$

For the cover-plate system, where $\phi = 0$,

$$\Theta' = 2\beta_{p'}\left(\frac{r_1}{r_2}\right)^2 - 1 \qquad (10)$$

If $\beta_{p'}(r_1/r_2)^2$ is kept the same for both systems (that is, the inlet angular momentum is the same), and if there is no disc-cooling flow, then the effectiveness of both systems will be the same. *Equation (8) holds for all adiabatic systems whether the flow is laminar, turbulent or inviscid and whether the flow is compressible or incompressible.*

El-Oun and Owen (1989) used an "unmixed theory" (where $\phi = 0$) for the adiabatic effectiveness of a direct-transfer pre-swirl system (where $r_1 = r_2$). Their theory was based on the Reynolds analogy in which the work was transferred by shear stresses in the boundary layer on the disc. If a fluid is brought to rest, or to the speed of a moving surface, by viscous shear then the adiabatic surface temperature is related to the total temperature of the fluid by a recovery factor, R, say. For the case where R = 1, when viscous recovery and isentropic recovery are identical, equation (8) becomes identical to the equation derived by El-Oun and Owen.

Although pressure losses do not affect the pre-swirl effectiveness directly, in practice they will reduce the amount of swirl that can be imparted to the air when the overall pressure drop in the system is fixed by engine conditions. The pressure loss in the pre-swirl nozzles is expected to increase with the square of the tangential velocity at inlet, and this loss will therefore be much larger in the cover-plate system, thereby reducing the inlet swirl ratio. However, as shown above, when disc-cooling air is introduced, the effectiveness of the direct-transfer system will be reduced. It is therefore unclear which of these two systems has the better adiabatic performance in practice.

Whatever the relative adiabatic performance, the effects of heat transfer and hot gas ingress are likely to increase significantly the temperature of the blade-cooling air in gas turbines. However, the adiabatic effectiveness provides a datum from which to measure the performance of all practical pre-swirl systems.

2.2 Source region in a rotating cavity with radial outflow

In a rotating cavity with a radial outflow of air, there is a source region where angular momentum is conserved and the incoming flow is entrained into boundary layers on the two discs. If the incoming flow is rotating faster than the disc ($\beta > 1$) then there will be radial inflow in the boundary layers; radial outflow in the boundary layers will only occur at the larger radii where $\beta < 1$. For free-vortex flow, rV_ϕ is constant, and if

$$\beta_{p'} = \frac{V_{\phi 1'}}{\Omega r_1} \qquad (11)$$

it follows that

$$\frac{V_\phi}{\Omega r} = \beta_{p'}\left(\frac{r_1}{r}\right)^2 = \beta_{p'}\left(\frac{x_1}{x}\right)^2 \qquad (12)$$

Equation (12) will be referred to as the equation for an "ideal free vortex".

If $\beta_{p'} > 1$, there will be a radius, $r = r_s$, say, where $V_\phi/\Omega r = 1$. It follows from equation (12) that

$$r_s = \beta_{p'}^{1/2}\, r_1 \qquad (13)$$

For $r > r_s$, air is entrained into the outflowing boundary layers until, at $r = r_e$, say, the entire mass flow rate, m_b, has been entrained. For $r > r_e$, nonentraining Ekman-type layers are formed and angular momentum in the core is no longer conserved; the radius r_e therefore corresponds to the edge of the source region.

It is useful to estimate the value of r_e which, according to Owen and Rogers (1995), will depend on the turbulent flow parameter, $\lambda_{T,b}$ and on $\beta_{p'}$. They proposed the following theoretical correlation for the nondimensional radial extent of the source region x_e :

$$\left(\frac{x_s}{x_e}\right)^{2.35} + \left(\frac{x_{e,o}}{x_e}\right)^{1.57} = 1 \qquad (14)$$

where $x_{e,o}$ is the value of x_e for the case where the flow enters with zero swirl ($\beta_{p'} = 0$). The value of $x_{e,o}$ is based on the free-disc entrainment rate, where

$$x_{e,o} = 1.375\, \lambda_{T,b}^{5/13} \qquad (15)$$

for the case where the flow is entrained equally into the boundary layers on both discs. The value of x_s in equation (14) is given from equation (13) where

$$x_s^2 = \beta_{p'}\, x_p^2 \qquad (16)$$

Equation (14) is only valid for $x_s < 1$ and for $x_e < 1$. It is easy to show that $x_e = 1$ when

$$\lambda_{T,b} = 0.437\,(1 - (\beta_{p'}\, x_p^2)^{1.18})^{1.66} \qquad (17)$$

providing $\beta_{p'}\, x_p^2 < 1$. For $\lambda_{T,b}$ greater than this value, the source region will fill the entire cavity and free-vortex flow will occur between the pre-swirl nozzles and blade-cooling passages. If $\beta_{p'} x_p^2 > 1$, there will be radial inflow in the boundary layers, with associated recirculating flow throughout the cavity. For most engine-operating conditions, it is expected that $\beta_{p'}\, x_p^2 < 1$ and that $\lambda_{T,b}$ will be greater than the value given by equation (17).

3 COMPUTIONAL MODEL

The steady-state, axisymmetric finite-volume solver used in this work is the same as that described by Wilson, Pilbrow and Owen (1995) for a related study of a direct-transfer pre-swirl rotor-stator system. The Launder-Sharma low-Reynolds-number k-ε turbulence model was used to close the coupled system of Reynolds-averaged Navier-Stokes and energy equations, and the flow was assumed to be incompressible. Turbulent heat transfer was represented using a turbulent Prandtl number Pr_T equal to 0.9. A staggered grid was used with the axial and radial velocity components stored mid-way between the grid points, where the other solution variables were located (pressure, tangential velocity, turbulence kinetic energy and dissipation rate, and total enthalpy). The cover-plate and inner shroud (Fig. 1b) were represented by block obstructions within the

computational grid and the equations were solved using the SIMPLEC pressure-correction algorithm.

The inlet nozzles and blade-cooling holes of the experimental rig were represented in the axisymmetric model by equivalent-area annular slots on the stator and rotor, with centrelines at $r = r_p$ and $r = r_b$ respectively. The axial velocity V_z of the pre-swirl air was assumed uniform at inlet and deduced from the prescribed mass flow rate m_p. Similarly, the axial velocity at the blade-cooling slot and the radial velocity at the outer seal were calculated from known mass flow rates m_b and m_s respectively; global mass balance was achieved by ensuring that $m_p = m_b + m_s$. The inlet tangential velocity $V_{\phi,p}$ was fixed to give the required swirl ratio β_p, and Neumann (zero normal derivative) boundary conditions for V_ϕ were used at the two outlets. The remaining velocity components at flow boundaries were taken to be zero, and no-slip conditions were applied at all solid surfaces. For the computations of the adiabatic effectiveness, the static temperature was prescribed at inlet, and Neumann conditions were applied elsewhere.

The Launder-Sharma turbulence model required a very fine grid near the boundaries, with $y+ < 0.5$ for the near-wall grid nodes, and the grid-spacing increased geometrically away from walls (including the cover-plate and shroud) with expansion factors of about 1.2. In total, a 223 by 223 axial by radial grid was used, with eight points covering each of the inlet and blade-cooling slots. About 55 axial grid nodes were within the cover-plate, with the remaining points divided equally between the rotor-stator system and the rotating cavity: about 70 radial grid points covered the annular pre-swirl chamber (Fig. 1b). Convergence of the iterative method was improved using the Gosman distributive damping term and a fixed V-cycle multigrid algorithm (Vaughan et al, 1989). Computation times were typically around 12 hours on a Silicon Graphics R10000 processor.

4 EXPERIMENTAL APPARATUS

A schematic diagram of the rig is shown in Fig 1. The direct-transfer rig (from which the present version was adapted) is described by Wilson et al (1995), and so only the salient details of the cover-plate rig are described here.

The outer radius of the system, b, was approximately 207mm, and the radial location of the pre-swirl nozzles and blade-cooling holes were $r_p = 90$ mm and $r_b = 200$ mm. There were 19 pre-swirl nozzles of 7.92 mm diameter, angled at 20^o to the tangential direction, and 60 blade-cooling holes of 7.7 mm diameter, with their axes normal to the disc. The axial spacing between the cover-plate, which was 5mm thick, and the stator was 10 mm, and between the cover-plate and the rotor disc the spacing was also 10 mm. The inner and outer radii of the annular pre-swirl chamber were $r_i = 80$ mm and $r_o = 100$ mm, and air entered the rotating cavity through the clearance at the centre of the cover-plate.

The cover-plate was made from transparent polycarbonate, and there was a window in the stator to provide optical access for LDA measurements in the rotating cavity between the cover-plate and the disc. Axial restraint of the cover-plate was provided by six cylindrical spacers of 12 mm diameter bonded to the cover-plate and to the disc at a mean radius of 142 mm. (For an inlet swirl ratio of $\beta_p = 2.5$, the design condition, free vortex flow would make $\beta = 1$ at $r = 142$ mm; at this radius, the spacers should cause the minimum of disturbance to the designed flow. When $\beta_p < 2.5$, the drag exerted by the spacers will tend to increase the angular momentum of the air for $r > 142$ mm)

The mass flow rates of the pre-swirl, blade-cooling and sealing flow, m_p, m_b and m_s, respectively, could be independently controlled, and the flow rates were measured, with an uncertainty of ± 3%, by orifice plates made to British Standards (BS1042). The rotor assembly could be rotated up to 7000 rev/min by a variable-speed electric motor, and the speed could be measured with an uncertainty of ± 1 rev/min. (For the tests conducted on this rig, a speed of 7000 rev/min corresponds to $Re_\phi \cong 2 \times 10^6$.)

It should be pointed out that, for the results presented below, the ideal swirl ratio, $\beta_{p'}$, was used (see Section 2). This was based on the measured mass flow rate, m_p, and the continuity equation: knowing the angle and diameter of the pre-swirl nozzles, $\beta_{p'}$ could be calculated.

The LDA measurements were made using a TSI back-scatter optical system with a Bragg-cell frequency shift and a single-channel IFA-750 burst correlator. A Spectra-Physics 4W argon-ion laser was used, and for the tests reported here up to 350 mW on the green line (514.5 nm) was used to measure the tangential component of velocity, V_ϕ, in, or near, the mid-plane of the rotating cavity for $0.57 < x < 1$.

The processor could handle Doppler frequencies up to 90 MHz with signal-to-noise ratios as low as -5dB. The beam spacing was 50 mm, and a converging lens with a focal length of 250 mm produced an optical probe volume 340μm long and 34μm diameter. The inlet air was seeded with micron-sized oil particles produced by a TSI 9306 six-jet atomiser. From these measurements, and those made using this LDA equipment in other rotating-disc rigs (see, for example, Gan *et al* 1996), the uncertainty in the measured values of $V_\phi / \Omega r$ is expected to be approximately ± 1%.

Velocity measurements were made over the following ranges of nondimensional parameters :

$5.3 \times 10^5 < Re_\phi < 1.25 \times 10^6$
$6500 < C_{w,b} < 26000$
$0.173 < \lambda_{T,b} < 0.363$
$1.18 < \beta_{p'} < 2.5$

5 COMPUTATION AND MEASUREMENTS

5.1 Flow structure

Figs 3 and 4 show the computed streamlines and contours of $V_\phi / \Omega r$ for $\lambda_{T,b} = 0.178$ and $\beta_{p'} = 1.27$ and for $\lambda_{T,b} = 0.229$ and $\beta_{p'} = 2.51$, respectively. The geometry corresponds to the experimental rig described in Section 4.

Values of Re_ϕ, $C_{w,b}$, $C_{w,p}$, $\lambda_{T,b}$ and β_p are given in the legends of Fig. 3 and 4; the nondimensional flow rate of the disc-cooling air, $C_{w,d}$, can be found from the difference between $C_{w,p}$ and $C_{w,b}$. The flow structure in the rotating cavity is determined by the magnitude of Re_ϕ, $\lambda_{T,b}$ and β_p; the magnitude of $C_{w,d}$ has an insignificant effect on

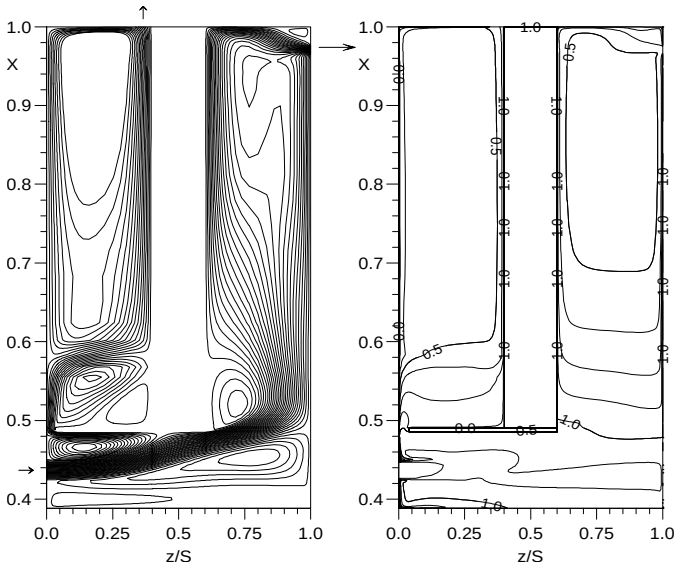

a) streamlines b) contours of $V_\phi/\Omega r$

Fig. 3 Computed flow structure for cover−plate system:
$Re_\phi = 1.09 \times 10^6$, $C_{w,b} = 1.21 \times 10^4$,
$C_{w,p} = 1.55 \times 10^4$, $\lambda_{T,b} = 0.178$, $\beta_{p'} = 1.27$

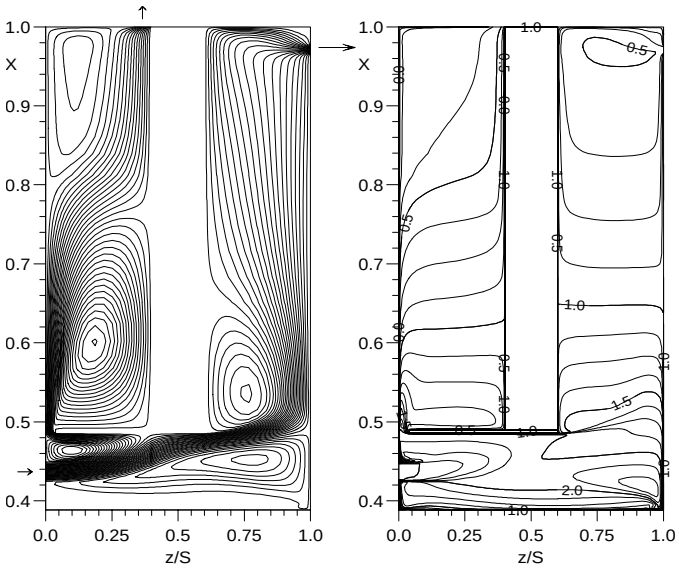

a) streamlines b) contours of $V_\phi/\Omega r$

Fig. 4 Computed flow structure for cover−plate system:
$Re_\phi = 0.553 \times 10^6$, $C_{w,b} = 0.902 \times 10^4$,
$C_{w,p} = 1.55 \times 10^4$, $\lambda_{T,b} = 0.229$, $\beta_{p'} = 2.51$

the flow in the rotating cavity although it obviously has a strong effect on that in the rotor-stator system.

Fig 3a shows the computed streamlines in three regions : the rotor-stator system (on the left-hand side of the figure); the rotating-cavity (on the right-hand side); and the pre-swirl annulus (near the bottom). In the rotor-stator system, there is a source region for $x < 0.6$, radially outward of which there is the expected radial outflow on the rotating cover-plate and inflow on the stator, with a core of rotating fluid between the two boundary layers. The flow in rotor-stator systems is well understood and will not be discussed further here.

The pre-swirl flow enters the system at $z/s = 0$ and $x = 0.44$ with a swirl ratio of $\beta_{p'} = 1.27$. There are recirculation zones on either side of the swirling jet with a stagnation point on the outer wall of the pre-swirl annulus ($x = 0.49$, $z/s \cong 0.42$). For $z/s < 0.42$, there is an axial flow in the outer boundary layer towards the pre-swirl nozzles. It is this flow that enters the rotor-stator system through the clearance between the outer annular wall and the stator.

Most of the pre-swirl flow enters the rotating cavity, impinging on the rotating disc and separating from the cover-plate: the separation zone extends to $x \cong 0.57$. For $x < 0.75$, there is a source region, radially outward of which the flow divides into two nonentraining Ekman-type layers. (For $\lambda_{T,b} = 0.178$ and $\beta_{p'} = 1.27$, equation (14) gives $x_e = 0.87$, which overestimates the size of the source region shown in Fig 3a.) The flow leaves the rotating cavity through the annular slot in the rotating disc, at $x = 0.97$, half the flow coming from the boundary layer on the disc and the other half from the boundary layer on the cover-plate via the peripheral shroud.

Fig 3b shows the contours of $V_\phi/\Omega r$ for this case. For $x > 0.57$, radially outward of the separation zone, there is little axial variation of V_ϕ outside the boundary layers on the two discs.

Fig 4a shows the computed streamlines for $\lambda_{T,b} = 0.229$ and $\beta_{p'} = 2.51$. In the rotating cavity, the separation zone is larger than that shown in Fig 3a and the source region extends throughout most of the cavity. (For $\beta_{p'} = 2.51$, equation (17) gives $\lambda_{T,b} = 0.173$; for $\lambda_{T,b} > 0.173$ the source region should fill the cavity, as shown in Fig 4a.)

Fig 4b shows that $V_\phi/\Omega r = 1$ at $x \cong 0.65$, which coincides with the edge of the separation zone on the cover-plate. For $x > 0.65$, there is little axial variation of V_ϕ outside the boundary layers on the discs.

Fig 5 shows the variation of $V_\phi/\Omega r$ with x^{-2} for three sets of $\lambda_{T,b}$ and $\beta_{p'}$. It is instructive to plot results against x^{-2} as free-vortex flow can be identified by straight lines passing through the origin at $x^{-2} = 0$. The "ideal free vortex", which corresponds to equation (12), is plotted from $x^{-2} = 0$ to $x^{-2} = 5.24$, the latter value being the radial location of the pre-swirl nozzles. The experimental measurements were obtained from nine tests carried out over many days. The nondimensional parameters varied slightly from test to test, but the nominal values indicated on the figure are accurate to around $\pm$ 2%.

The "computed free vortex" in Fig 5 is a free-vortex curve drawn through the computed values of $V_\phi/\Omega r$ at a single radius; a value of $x^{-2} = 2.2$ was arbitrarily chosen. The "computed free vortex" shows the radial extent to which the results conform to a free vortex. It is also possible to compute the "effective pre-swirl ratio", $\beta_{p,eff}$, corresponding to the value of the computed free vortex at $x^{-2} = 5.24$. Also shown on Fig 5 are the locations of the centres of the blade-cooling slot, at $x^{-2} = 1.06$, and the cover-plate supports, at $x^{-2} = 2.13$.

Referring to Fig 5a, where $\beta_{p'} = 1.25$ and $\lambda_{T,b} = 0.18$, the computations show free-vortex flow from $1.8 < x^{-2} < 4$ ($0.5 < x < 0.75$) with $\beta_{p,eff} \cong \beta_{p'}$. The shear near $x = 1$ is associated with the boundary layer on the shroud, and the departure from the

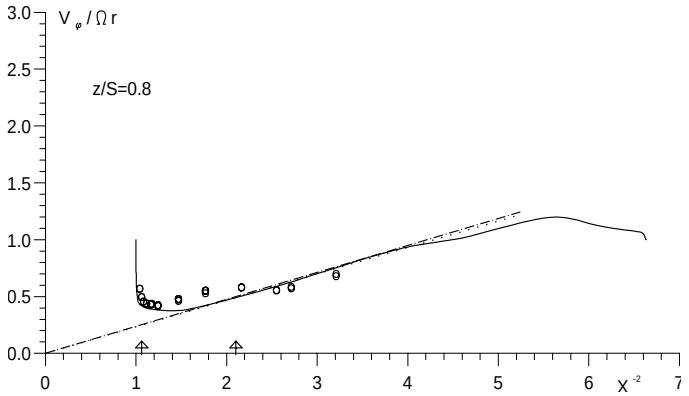

a) $\beta_{p'} = 1.25$, $\lambda_{T,b} = 0.18$, $Re_\phi = 1.23 \times 10^6$

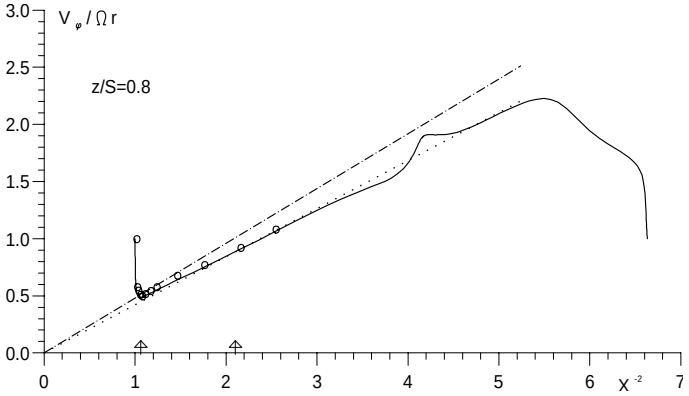

b) $\beta_{p'} = 2.5$, $\lambda_{T,b} = 0.23$, $Re_\phi = 0.55 \times 10^6$

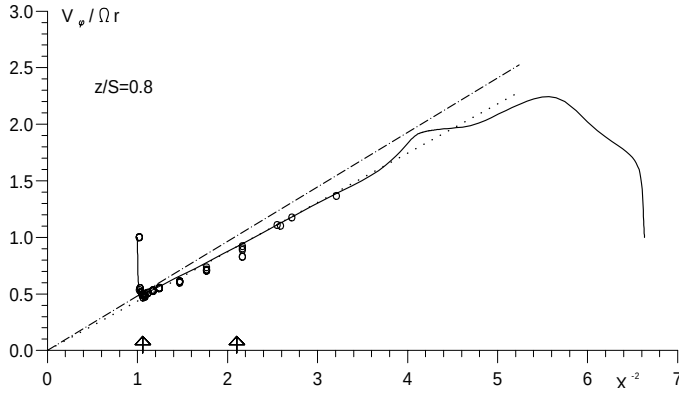

c) $\beta_{p'} = 2.5$, $\lambda_{T,b} = 0.36$, $Re_\phi = 0.55 \times 10^6$

Fig 5 Comparison between computed and measured variation of $V_\phi/\Omega r$ with x^{-2}

o	experimental data;
———	computation;
– · –	ideal free vortex;
.....	computed free vortex;
↑	centre of blade-cooling slot;
↑	centre of cover-plate support

free-vortex curve at $x^{-2} \cong 1.8$ corresponds to the edge of the source region, which was discussed above. (It should be noted that angular momentum is not conserved outside the source region in the core flow between Ekman-type layers - see Owen and Rogers, 1995.)

The experimental data shown in Fig 5a are consistent with a free vortex at the larger values of x^{-2} and illustrate the shear in the boundary layer near x = 1. Downstream of the cover-plate supports, the measurements show an increase in V_ϕ above the ideal free-vortex curve. In this region, where $V_\phi/\Omega r \tilde{} 0.5$, the supports have evidently imparted angular momentum to the fluid, as suggested in Section 4.

In Fig 5b, where $\beta_{p'} = 2.5$ and $\lambda_{T,b} = 0.23$, the computations and measurements lie on a free-vortex curve that is significantly lower than the ideal one. For this case, where $V_\phi/\Omega r \cong 0.9$ near the cover-plate supports, the supports appear to have no significant effect on the flow. For these values of $\beta_{p'}$ and $\lambda_{T,b}$, the source region fills the entire cavity, and the computed and measured values of $V_\phi/\Omega r$ show that free-vortex behaviour occurs up to the edge of the boundary layer on the shroud at x = 1.

Fig 5c, where $\beta_{p'} = 2.5$ and $\lambda_{T,b} = 0.36$, shows computed and measured results similar to those in Fig 5b. These results illustrate the fact that $\beta_{p'}$ is the dominant parameter as far as $V_\phi/\Omega r$ is concerned, although $\lambda_{T,b}$ does have an effect on the size of the source region. The measurements and computations for results that are not shown here suggest that, for a fixed value of $\lambda_{T,b}$, the ratio of $\beta_{p,\,eff} / \beta_{p'}$ decreases significantly as $\beta_{p'}$ increases; for a fixed value of $\beta_{p'}$, the ratio increases as $\lambda_{T,b}$ increases.

5.2 Pre-swirl effectiveness

Fig 6 shows a comparison between the computed values of Θ, using the definition in equation (7), and the theoretical curve for Θ', using equation (10). The geometry was based on the rig described in section 4 where $r_1/r_2 = 0.45$.

It should be pointed out that the authors were unable to make any reliable experimental measurement of Θ for the adiabatic case. Although total temperature probes were fitted in the rig to measure T_{01} and T_{t2}, it was not possible to conduct experiments under adiabatic conditions. Unlike the rig used by El-Oun and Owen (1989), the one used here was designed for heat-transfer experiments. Windage heating from the heater assembly and heat input from the bearings created heat transfer from the disc to the cooling air even when no external heating was used. Heat transfer results, and the measurement of the temperature of the blade-cooling air, will be the subject of a subsequent paper.

Fig 6 shows good agreement between the computed and theoretical variation of Θ with $\beta_{p'}$ in the range $\beta_{p'} = 0$ to 4.60. It is convenient to define a nondimensional error, e_Θ, based on the difference between Θ' and Θ. From equation (7) it follows that

$$e_\Theta = \Theta' - \Theta = \frac{c_p (T_{t,2} - T_{t,2}')}{\frac{1}{2}\Omega^2 r_2^{\,2}} \qquad (18)$$

where $T_{t,2}'$ is the theoretical value of the blade-cooling temperature, based on equation (10), and $T_{t,2}$ is the computed value. For 15 computed values, e_Θ range from 10^{-4} (for $\beta_{p'} = 2.5$) to 0.019 (for $\beta_{p'} = 4.6$). As the theoretical value given in equation (10) is exact, e_Θ represents the magnitude of the numerical errors in the computed values of Θ.

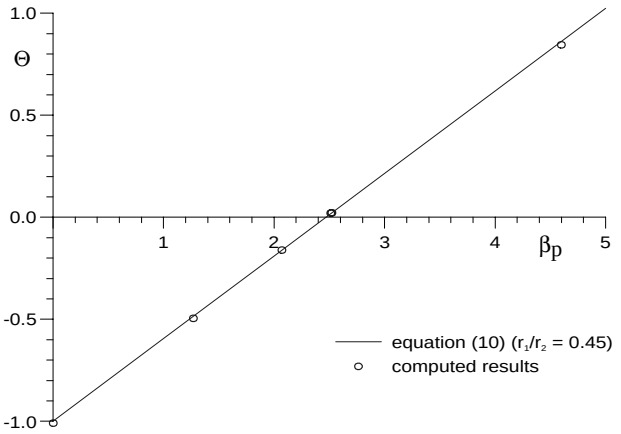

Fig. 6 Comparison between computed and theoretical variation of Θ with β_p

For the experimental rig, the above conditions correspond to $\Omega r_2 < 84$ m/s, and the "dynamic temperature" ($\Omega^2 r_2^2/2c_p$) is less than 3.5°C; a value of $e_\Theta = 0.019$ therefore corresponds to 0.07°C in the rig. In an engine, where dynamic temperatures can be in excess of 50°C, a value of $e_\Theta = 0.019$ would correspond to around 1°C. For practical purposes, the agreement between the computed and theoretical values of Θ can be regarded as satisfactory.

In engines, the effectiveness of cover-plate systems will be reduced by heat transfer from the turbine disc to the cooling air. For direct-transfer systems, the ingestion of disc-cooling air and mainstream gas into the blade-cooling passages is likely to have an even greater effect on the temperature of the blade-cooling air. However, even when heat transfer is significant, the adiabatic effectiveness provides a useful datum from which to measure pre-swirl performance.

6 CONCLUSIONS

Computations, made using an elliptic solver incorporating the Launder-Sharma low-Reynolds-number turbulence model, and velocity measurements, made using an LDA system in a purpose-built experimental rig, have been used to study the flow in an adiabatic cover-plate system.

The computations confirm that the flow between the cover-plate and the rotating disc is similar to that in a rotating cavity with a radial outflow of air. For sufficiently large values of $\lambda_{T,b}$, the source region fills most of the cavity and, outside the boundary layers, the flow behaves as a free vortex. The agreement between the measured and computed values of $V_\phi/\Omega r$ in the rotating cavity is mainly very good. Supports, attached to the cover-plate on the experimental rig, could disturb the flow when $V_\phi < \Omega r$ in the vicinity of the supports; at the design pre-swirl ratio ($\beta_{p'} = 2.5$), the effect of the supports was insignificant. The computed values of $V_\phi/\Omega r$ approximated to a free vortex with an effective pre-swirl ratio of $\beta_{p,eff}$. For $\beta_{p'} > 1.25$, the ratio of $\beta_{p,eff}/\beta_{p'}$ is less than unity and it decreases as $\beta_{p'}$ increases.

Values of the computed nondimensional pre-swirl effectiveness, Θ, were compared with theoretical values, Θ', obtained from a thermodynamic analysis of an adiabatic system. The analysis shows that Θ' depends only on the parameter $\beta_{p'}(r_p/r_b)^2$, and for $r_p/r_b = 0.45$ and $0 \le \beta_{p'} \le 4.6$ the error between Θ' and Θ was less than 2% of the "dynamic temperature", $\Omega^2 r_b^2/2c_p$.

ACKNOWLEDGEMENTS

The authors thank the Engineering and Physical Sciences Research Council and European Gas Turbines Ltd for funding the research described in this paper, and the Turkish Government and Kocaeli University for providing the financial support for Hasan Karabay. We also wish to thank the reviewers for their constructive comments.

REFERENCES

Chen, J., Owen, J.M. and Wilson, M, 1993a. Parallel-computing techniques applied to rotor-stator systems: fluid dynamics computations, in Numerical Methods in Laminar and Turbulent Flow, 8, 899 - 911 (Pineridge Press, Swansea).

Chen, J., Owen, J.M. and Wilson, M, 1993b. Parallel-computing techniques applied to rotor-stator systems: thermal computations, in Numerical Methods in Thermal Problems, 8, 1212 - 1226, (Pineridge Press, Swansea).

El-Oun, Z and Owen, J.M., 1989. Pre-swirl blade-cooling effectiveness in an adiabatic rotor-stator system. J. Turbomachinery, 111, 522 - 529.

Gan, X., Mirzaee, I., Owen, J.M., Rees, D.A.S. and Wilson, M., 1996. Flow in a rotating cavity with a peripheral inlet and outlet of cooling air. ASME Int. Gas Turbine and Aero Engine Congress, Birmingham, UK, 10-13 June 1996. ASME Paper No 96-GT-309.

Meierhofer, B. and Franklin, C.J. , 1981. An investigation of a preswirled cooling airflow to a gas turbine disk by measuring the air temperature in the rotating channels. ASME Int. Gas Turbine Conf., Houston, Paper No 81-GT-132.

Owen, J.M. and Rogers, R.H., 1989. Flow and heat transfer in rotating disc systems: Vol. 1: Rotor-stator systems. Research Studies Press, Taunton, UK and John Wiley, New York, USA.

Owen, J.M. and Rogers, R.H., 1995. Flow and heat transfer in rotating disc systems: Vol. 2: Rotating cavities. Research Studies Press, Taunton, UK and John Wiley, New York, USA.

Popp, O., Zimmermann, H. and Kutz, J., 1996. CFD analysis of coverplate receiver flow. ASME Int. Gas Turbine and Aeroengine Cong., Birmingham, UK. Paper No. 96-GT-357.

Vaughan, C.M., Gilham, S. and Chew, J.W., 1989. Numerical solutions of rotating disc flows using a non-linear multigrid algorithm. Proc. 6th Int. Conf. Num. Meth. Laminar Turbulent Flow, pp 66-73, (Pineridge Press, Swansea).

Wilson, M., Pilbrow, R.G. and Owen, J.M., 1995. Flow and heat transfer in a pre-swirl rotor-stator system. ASME Int. Gas Turbine and Aeroengine Congress, Houston, June 1995. Paper No 95-GT-239.